

Identification of a human splenic marginal zone B cell precursor with NOTCH2-dependent differentiation properties

Marc Descatoire,¹ Sandra Weller,¹ Sabine Irtan,² Sabine Sarnacki,² Jean Feuillard,^{3,4} Sébastien Storck,¹ Anne Guiochon-Mantel,^{5,6} Jérôme Bouligand,^{5,6} Alain Morali,⁷ Joseph Cohen,⁸ Emmanuel Jacquemin,^{8,9} Maria Iascone,¹⁰ Christine Bole-Feysot,¹¹ Nicolas Cagnard,¹² Jean-Claude Weill,¹ and Claude-Agnès Reynaud¹

¹Institut Necker-Enfants Malades, INSERM U1151-CNRS UMR 8253, Sorbonne Paris Cité, Université Paris Descartes, Faculté de Médecine-Site Broussais, 75014 Paris, France

²Service de Chirurgie Pédiatrique, Hôpital Necker-Enfants-Malades, Université Paris Descartes, 75015 Paris, France

³Unité Mixte de Recherche CNRS 7276, Faculté de Médecine, 887025 Limoges, France

⁴Centre Hospitalier Universitaire Dupuytren, Laboratoire d'Hématologie, 87042 Limoges, France

⁵INSERM Unité Mixte de Recherche S693, Université Paris Sud, Faculté de Médecine Paris-Sud, 94276 Le Kremlin-Bicêtre, France

⁶AP-HP, Hôpital de Bicêtre, Service de Génétique Moléculaire, Pharmacogénétique, et Hormonologie, 94275 Le Kremlin-Bicêtre, France

⁷Hépatologie et gastro-entérologie pédiatriques, Hôpital d'enfants, INSERM U954, CHU de Nancy-Brabois, 54511 Vandoeuvre-lès-Nancy, France

⁸Hépatologie Pédiatrique and Centre de Référence National de l'Atrésie des Voies Biliaires, Hôpital Bicêtre, AP-HP and Université Paris-Sud 11, 94275 Le Kremlin-Bicêtre, France

⁹INSERM U757, Université Paris-Sud 11, 91405 Orsay, France

¹⁰Molecular Genetics Laboratory, AO Papa Giovanni XXIII, 24127 Bergamo, Italy

¹¹Plateforme de génomique de la fondation Imagine, Hôpital Necker, 75015 Paris, France

¹²Plateforme de bioinformatique de l'université Paris Descartes, 75015 Paris, France

Mouse splenic marginal zone precursors (MZPs) differentiate into marginal zone B (MZB) cells under a signaling pathway involving Notch2 and its ligand, delta-like 1 ligand (DLL1). We report the identification of an MZP subset in the spleen of young children. These MZPs differentiate into MZ-like B cells in vitro in the presence of OP9 cells expressing human DLL1, as demonstrated by the up-regulation of classical MZB cell markers. A set of diagnostic genes discriminating IgM⁺IgD⁺CD27⁺ blood and splenic MZB cells from switched B cells was identified (up-regulation of *SOX7*, down-regulation of *TOX*, *COCH*, and *HOPX*), and their expression during the induction assay mirrored the one of MZB cells. Moreover, Alagille patients with a *NOTCH2* haploinsufficiency display a marked reduction of IgM⁺IgD⁺CD27⁺ B cells in blood, whereas their switched memory B cells are not affected. Altogether, these results argue in favor of the existence of a rodent-like MZB cell lineage in humans.

CORRESPONDENCE

Claude-Agnès Reynaud:
claude-agnes.reynaud@inserm.fr
OR

Jean-Claude Weill:
jean-claude.weill@inserm.fr

Abbreviations used: DLL1, delta-like 1 ligand; GC, germinal center; MNC, mononuclear cell; MTG, MitoTracker green; MZB, marginal zone B; MZP, marginal zone precursor.

The rodent marginal zone B (MZB) cell population represents a distinct B cell lineage that resides in the MZ of the spleen. These MZB cells bear an unmutated BCR and are in a pre-activated state, allowing them to respond rapidly to challenge by bloodborne T cell-independent antigens (Martin and Kearney, 2002). In contrast, the existence of an equivalent MZB cell subset in humans remains controversial. Why is this so? B cells with a similar surface Ig phenotype (IgM^{high}IgD^{low}) are found in the human splenic MZ, but they display the CD27⁺ marker and mutated immunoglobulin genes, and have

been accordingly considered as post-germinal center (GC) memory B cells (Dunn-Walters et al., 1995; Tangye et al., 1998; Zandvoort et al., 2001). However, patients who have crippling mutations in the CD40 or CD40L gene, mutations which prevent formation of GCs and of switched memory B cells, still possess a circulating IgD⁺ IgM⁺CD27⁺ mutated subset (Weller et al., 2001).

© 2014 Descatoire et al. This article is distributed under the terms of an Attribution-Noncommercial-Share Alike-No Mirror Sites license for the first six months after the publication date (see <http://www.rupress.org/terms>). After six months it is available under a Creative Commons License (Attribution-Noncommercial-Share Alike 3.0 Unported license, as described at <http://creativecommons.org/licenses/by-nc-sa/3.0/>).

It was thus proposed that, in humans, IgD⁺IgM⁺CD27⁺ B cells recirculate and diversify their BCR by hypermutation outside GCs (Weller et al., 2001, 2004). Moreover, IgD⁺IgM⁺CD27⁺ B cells, either in blood or spleen, do not show, as opposed to switched memory B cells, any sign of antigen-driven selection and expansion in young children <2 yr of age, in spite of the several vaccination episodes they experience (Weller et al., 2008). Because mutations on their BCR are observed before 2 yr, i.e., before immunological competence against T cell-independent antigens is acquired, it was proposed that human IgD⁺IgM⁺CD27⁺ B cells diversify their BCR along a developmental program outside any immune response, whether T cell-dependent or -independent. Based on these observations and on their MZ-like B cell phenotype (CD21^{high}, CD23^{low}, and CD1c^{high}), it was thus put forward that splenic and blood IgM⁺IgD⁺CD27⁺ B cells, which represent 15–20% of total B cells, are the human equivalent of the mouse MZ lineage (Weill et al., 2009). Their predominant role in the response to T cell-independent antigens, such as polysaccharides from encapsulated bacteria, was also suggested (Kruetzmann et al., 2003), and B cells with anti-pneumococcal polysaccharide specificity have been detected in this subset (Tsuiji et al., 2006).

Contradictory data have, however, been reported (Tangye and Good, 2007). First, switched and IgD⁺IgM⁺CD27⁺ B cells have been shown to be transcriptionally and phenotypically very close (Good and Tangye, 2007; Good et al., 2009). Second, clonal relationships between these two subsets were found when analyzed in blood, VDJ junctions being frequently shared between cells belonging to both populations (Seifert and Küppers, 2009). These results thus suggested that the majority, if not all, IgD⁺IgM⁺CD27⁺ B cells, or at least those present in blood, are in fact memory B cells responding to T cell-dependent antigens that left the GC reaction before switching to other isotypes.

MZ precursors (MZPs) were characterized in mice among splenic transitional B cells (Srivastava et al., 2005). Convincing in vivo experiments identified these immediate precursors at a differentiation stage after transitional T2 cells, whereas T2 cells were still able to give rise to both follicular and MZB cells. Moreover it was proposed that mouse transitional B cells could show some capacity to differentiate into MZB cells in vitro, under a Notch2 stimulation mediated by the Delta-like 1 ligand (Dll1; Roundy et al., 2010). This experiment was in agreement with in vivo gene inactivation experiments showing that the Notch2–Dll1 pathway controlled the differentiation of splenic transitional B cells into MZB cells (Saito et al., 2003; Hozumi et al., 2004). A haploinsufficiency of either *Notch2* or *Dll1* effectively induced a marked reduction of the MZB cell subset, and a complete B cell-restricted Notch2 deficiency abrogated its formation.

The transmembrane CD45 protein is expressed on all human hematopoietic cells, acting as a regulator of antigen receptor signaling through its tyrosine phosphatase activity. In T cells, several isoforms of CD45 are generated by alternate splicing, resulting in the expression of various combinations of

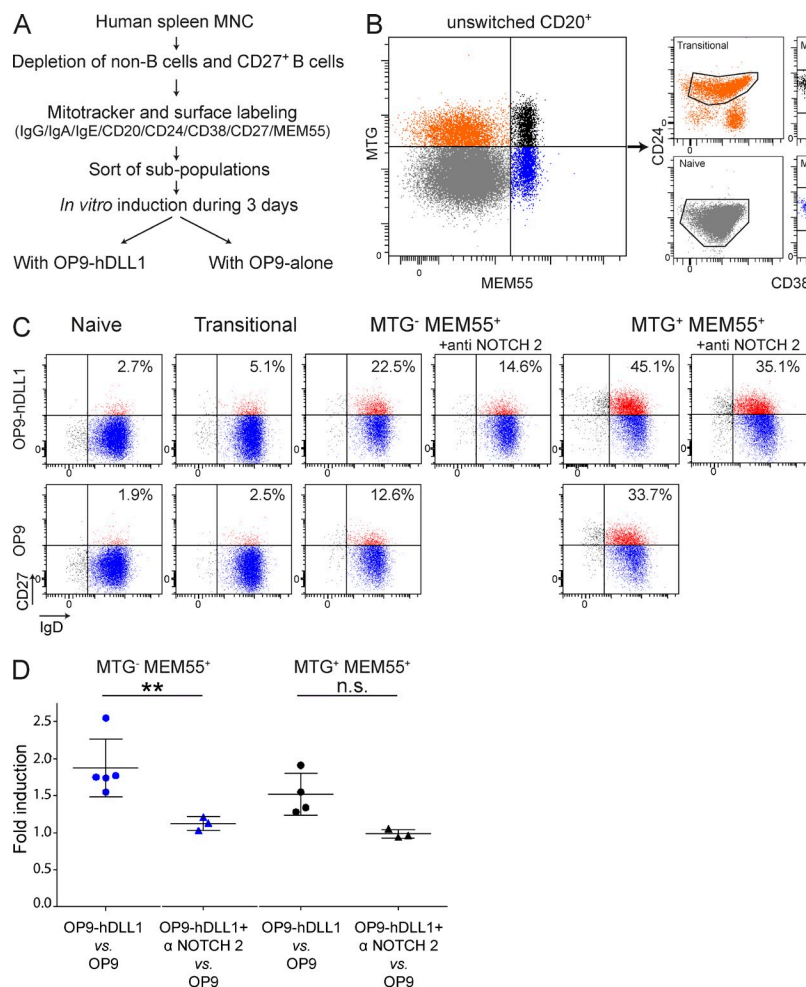
exons (RA, RB, and RC) and different N- and O-linked glycosylation patterns (Earl and Baum, 2008; Oberdoerffer et al., 2008). Such variants segregate with commitment to different effector fates, as well as with different antigen receptor signaling thresholds, although the precise molecular mechanism underlying this regulation is still not clear. Although the differential expression of various forms of CD45 has not been well studied in human B cells, Koethe et al. (2011) recently described a new epitope on CD45 characterized by the O-glycosylation of the CD45RB isoform and identified by the monoclonal antibody MEM-55. This epitope is not expressed on classical transitional and naive B cells but is highly expressed on switched CD27⁺ and CD27⁻ memory B cells, plasmablasts, and IgD⁺IgM⁺CD27⁺ B cells. Using this monoclonal antibody, these authors identified in blood a new MEM55⁺ B cell subset, which, as opposed to naive B cells, was IgM^{high} and ABCB1 transporter-negative but did not bear the classical transitional markers CD10 and CD38. This MEM55⁺ immature population was enlarged in blood in young children and in bone marrow-transplanted patients. Based on these data, the authors proposed that this new subset could be the precursor of naive B cells or immediate MZB cell precursors (Koethe et al., 2011; Bemark et al., 2012).

We define in this report an MZP population in spleen from young children that represents a new entity among this immature MEM55⁺ population because it expresses, like naive B cells and as opposed to all other human B cell subsets, the ABCB1 transporter. This new B cell fraction possesses the cardinal property of MZP, being able to differentiate in vitro into MZB cells under the NOTCH2–DLL1 signaling pathway. Moreover, patients suffering from an Alagille syndrome and with a heterozygous mutation in *NOTCH2* are shown to display a reduction of their circulating IgD⁺IgM⁺CD27⁺ B cells while their switched memory B cells are not affected. Altogether, these results argue in favor of the existence in humans of a bona fide MZB cell population, which differentiates, like its mouse counterpart, from a splenic MZP through a NOTCH2 signaling pathway.

RESULTS

MTG⁺MEM55⁺ and MTG⁻MEM55⁺ cells present in the spleen of young children are putative MZPs

B cells residing in the splenic MZ in humans are characterized by the surface phenotype CD27⁺IgD^{low}IgM^{high} (Tangye et al., 1998; Zandvoort et al., 2001; Weller et al., 2004). In mice, among different integrated signals, Notch2 signaling plays a key role in the differentiation of splenic transitional T2 cells into MZP that further differentiate into MZB cells (Pillai and Cariappa, 2009). To identify an MZP equivalent in humans, and by analogy with the mouse, we looked for a splenic B cell subset, present among CD27-negative cells, that would acquire an MZ-like phenotype (defined by the de novo expression of CD27) after a NOTCH2-dependent signal. Based on our previous observations that the frequency of immature B cells decline with age in the human spleen (Weill et al., 2009), we focused on spleen samples from young

**Figure 1. Identification of candidate**

MZPs from children spleen. (A) Isolation scheme of candidate MZP subsets from MNCs from children spleens (4–8 yr). (B) MTG and MEM55 (an antibody against a glycosylated variant of CD45RB) flow cytometry profiles of IgG⁻IgE⁻IgA⁻CD27⁻CD20⁺ cells revealed four distinct fractions that were isolated after the indicated CD24 and CD38 sort gates. (C) The four fractions isolated in B were co-cultured either with OP9 + hDLL1 or OP9 cells alone. After 3 d, cells were recovered, stained for CD20, IgD, and CD27, and CD20⁺-gated cells were analyzed for CD27 up-regulation. For MTG⁻MEM55⁺ and MTG⁺MEM55⁺ cells, the effect of a blocking anti-NOTCH2 mAb added in the OP9-hDLL1 cultures was evaluated. Percentages of IgD⁺CD27⁺ among total B cells after differentiation are indicated on each dot plot. Mean B cell survival after 3 d of culture was 19 ± 3% for both MEM55⁺ subsets. Experimental repeats (3 or 5 depending on the assay) are depicted in Table S1. (D) For the two MEM55⁺ subsets, a fold induction corresponding to the ratio of IgD⁺ cells becoming CD27-positive in the OP9-hDLL1 (with or without anti-NOTCH2 mAb) versus OP9 condition were plotted with indicated means ± SD (complete data from 5 different donors are listed in Table S1). Statistical significance is indicated on graphs as determined by paired, two-tailed Student's *t* test. **, *P* < 0.01; n.s., nonsignificant.

children between 4 and 8 yr of age, for which MZP may likely be present in a higher proportion. Transitional B cells in humans have been initially identified based on the high expression of CD10, CD24, and CD38 relative to mature B cell subsets (Sims et al., 2005; Cuss et al., 2006). Refined subsets of transitional B cells have been further delineated from naive cells using markers such as the ABCB1 transporter (which expression allows the extrusion of the Mitotracker green [MTG] fluorescent dye) or the recently described CD45RB isoform detected by the MEM55 mAb (Palanichamy et al., 2009; Koethe et al., 2011). We thus analyzed CD27-depleted splenic B cells that have been pulsed/chased with MTG and then labeled with anti-IgG, -IgA, -IgE, -CD20, -CD24, -CD38, and -CD27 Abs together with the MEM55 mAb (Fig. 1 A). Based on the staining with MTG and MEM55, four distinct IgG⁻IgA⁻IgE⁻CD27⁻CD20⁺ B cell populations were identified (Fig. 1 B): transitional cells (MTG⁺MEM55⁺), further separated from residual GC B cells by the CD38/CD24 marker, naive B cells (MTG⁻MEM55⁻), and the new MEM55⁺ B cell subset recently described in blood Koethe et al. (2011); surprisingly, and as opposed to their initial description, this latter subset included a clear population expressing the ABCB1 transporter (MTG⁻), previously known to be

uniquely expressed by naive B cells (Wirhth and Lanzavecchia, 2005). The four subsets were sorted and plated on OP9 stromal cells expressing or not human DLL1 (hDLL1), a NOTCH2 ligand. In some cases, anti-NOTCH1 or -NOTCH2 blocking antibodies were added to the sorted fractions cultured on OP9-hDLL1. After a 3-d culture, the up-regulation of CD27 was used as the main criteria of the differentiation of the initial cell fraction into MZ-like B cells. A fold induction corresponding to the ratios of IgD⁺ cells becoming CD27-positive in the OP9-hDLL1 (or OP9-hDLL1 + anti-Notch2) versus OP9 condition was plotted for each experiment. As shown (Fig. 1 C and Table S1), most naive B cells cultivated with either OP9-hDLL1 or OP9 cells alone retained their original CD27⁻ phenotype. The proportion of transitional B cells that acquired expression of CD27 in the OP9-hDLL1 culture (a mean of 9.5%) remained low in comparison to the one observed for MTG⁻MEM55⁺ and MTG⁺MEM55⁺ cells. Indeed, the proportion of cells that strongly up-regulated CD27 in the OP9-hDLL1 culture reached a mean of 22 ± 8% and 43 ± 7% for MTG⁻MEM55⁺ and MTG⁺MEM55⁺ cells, respectively (Fig. 1 C and Table S1). However, the fold induction was higher for MTG⁻MEM55⁺ cells than for MTG⁺MEM55⁺ cells, for which the proportion of induced CD27⁺

cells without a DLL1 signal was already quite high ($30 \pm 9.5\%$). For both subsets, the induction was inhibited by an anti-Notch2 blocking antibody added into the OP9-hDLL1 cell culture, whereas an anti-Notch1 antibody tested on MTG⁻MEM55⁺ cells had no effect (Fig. 1 C and Table S1). However, when comparing the fold induction values, the inhibition was statistically significant only for MTG⁻MEM55⁺ cells (Fig. 1 D). In conclusion, based on their ability to acquire an MZ-like surface phenotype under a NOTCH2/DLL1 signal, both MTG⁻MEM55⁺ and MTG⁺MEM55⁺ cells can be considered as putative MZPs. However, the higher proportion of MTG⁺MEM55⁺ cells having up-regulated CD27 in the absence of hDLL1 suggests that this subset may have already received a signal in vivo that would allow them to be at least partly independent from the NOTCH2 signal provided in vitro. This suggests also that MTG⁺MEM55⁺ might be at a more advanced differentiation stage toward MZB cells.

Other activation procedures have been reported which can induce CD27 expression on naive B cells. Two of them were tested on MTG⁻MEM55⁺ B cells: CD40L plus IL21, and SAC plus IL2. Both conditions were able to induce a large CD27⁺ fraction (55 and 75%, respectively). However, these CD27⁺ cells appear to be large, blastic B cells in which expression of *PRDM1* (encoding BLIMP1) was also induced (unpublished data). This is in marked contrast with B cells in OP9-DLL1 cultures, which did not undergo major changes in cell morphology and for which *PRDM1* expression remained at background levels (unpublished data), thus indicating that CD27 expression was acquired outside a plasma cell differentiation pathway in these specific culture conditions.

MTG⁻MEM55⁺ cells are MZP based on transcriptional, phenotypic, and Ig somatic hypermutation analysis

To further characterize MTG⁻MEM55⁺ and MTG⁺MEM55⁺ cells, the gene expression profiles of these two populations together with those of naive and MZB cells were determined by microarray analysis. The transcription profile of MZB and naive B cells differed for 1,855 probes, considering a twofold change and a *p*-value <0.05. According to the same criteria, the MTG⁻MEM55⁺ subset differed by 249 and 990 probes from naive and MZB cells, respectively, whereas the corresponding values for the MTG⁺MEM55⁺ subset were 750 probes compared with naive and 462 compared with MZB. To further determine the relationships between these four subsets, a principal component analysis was performed using the 1,855 probes that were differentially expressed between naive and MZB cells (Fig. 2 A). Unlike naive and MZB cells that appeared as rather homogeneous groups, MTG⁻MEM55⁺ and MTG⁺MEM55⁺ cells in particular were less tightly clustered. Nevertheless, both subsets displayed an intermediate gene profile between MZB and naive B cells, whereas MTG⁻MEM55⁺ cells were closer to naive cells and were thus the most distant subset from MZB cells in terms of transcriptional program. This suggests that MTG⁻MEM55⁺ cells represent an earlier differentiation stage than MTG⁺MEM55⁺ cells.

We next analyzed the frequency of somatic mutations on Ig genes of splenic MZB, MTG⁺MEM55⁺, and MTG⁻MEM55⁺ cells isolated from five different children (aged 4–6 yr; Fig. 2 B and Fig. S1). As expected, MZB cells from all the donors were already diversified with a mean mutation frequency of 1.74% and with 77% of the sequences being mutated. Interestingly, in both MTG⁺MEM55⁺ and MTG⁻MEM55⁺ cells, we could find mutated sequences, but both the range and the frequency of mutations were much lower (0.65 and 0.18%, respectively). Most of the sequences (88%) were unmutated in MTG⁻MEM55⁺ cells (except for one donor who also showed a much higher load of Ig mutations in its MZB compartment; Fig. S1), whereas the proportion of germline sequences was only 55% in the MTG⁺MEM55⁺ cell fraction. At the phenotypic level, MTG⁺MEM55⁺ B cells were similar to their MTG⁻ counterpart, apart from a few differences which make them closer to MZB (e.g., CD24 and CD200; Fig. 2 E). At the transcriptional level, the most striking difference, which discriminates them from all other splenic subsets, is the expression of *SOX5*, previously reported in FCRL4⁺CD27⁻ tissue memory B cells (Fig. 2 C; Ehrhardt et al., 2008). They also expressed CD27 at a low level, 10-fold over naive B cells (unpublished data), which might contribute to the higher CD27 induction observed in OP9 control cultures. Altogether, given its greater dependency to a NOTCH2 signal to differentiate into MZ-like B cells, its gene profile, and its almost nonmutated Ig status, the MTG⁻MEM55⁺ cell fraction appears as the earliest MZP characterized. As a consequence, MTG⁻MEM55⁺ will be referred to as MZP thereafter.

To gain further insights into a NOTCH2 signature that may be already present in MZP cells, we took advantage of a genome-wide expression analysis performed on an EBV-transformed human lymphoblastoid B cell line induced to express an activated NOTCH2 receptor (NOTCH2-IC; Kohlhof et al., 2009). Through data mining, a list of 1,678 and 1,453 genes that were, respectively, up- or down-regulated after 3 d of induction of the NOTCH2-IC was established (fold change ≥ 1.5). We then established a list of 369 genes that were differentially expressed between naive and MZP cells, with a similar fold change (≥ 1.5 ; *P* < 0.05). Both lists of genes were then compared, and genes in common are represented in the Venn diagrams shown in Fig. 2 D. Among the genes that distinguish MZP from naive cells, we already found a clear Notch2 signature because 44 out of the 215 up-regulated genes and 53 out of the 154 down-regulated genes were found in the listed genes that were, respectively, up- or down-regulated after activation of the Notch2 pathway. This signature nevertheless reflects a preliminary stage of induction because it lacks major NOTCH2 downstream effectors activated in the MZB subset like *DTX1* or *HES4*. It thus appears that MZP might have already received in vivo some activating signals of the NOTCH2 pathway upon their splenic localization. Interestingly, a Notch2 signature involving 88 genes (57 up-regulated and 31 down-regulated) was also observed for the genes differentially expressed in the MTG⁺MEM55⁺ subset compared with naive B cells, supporting the proposition

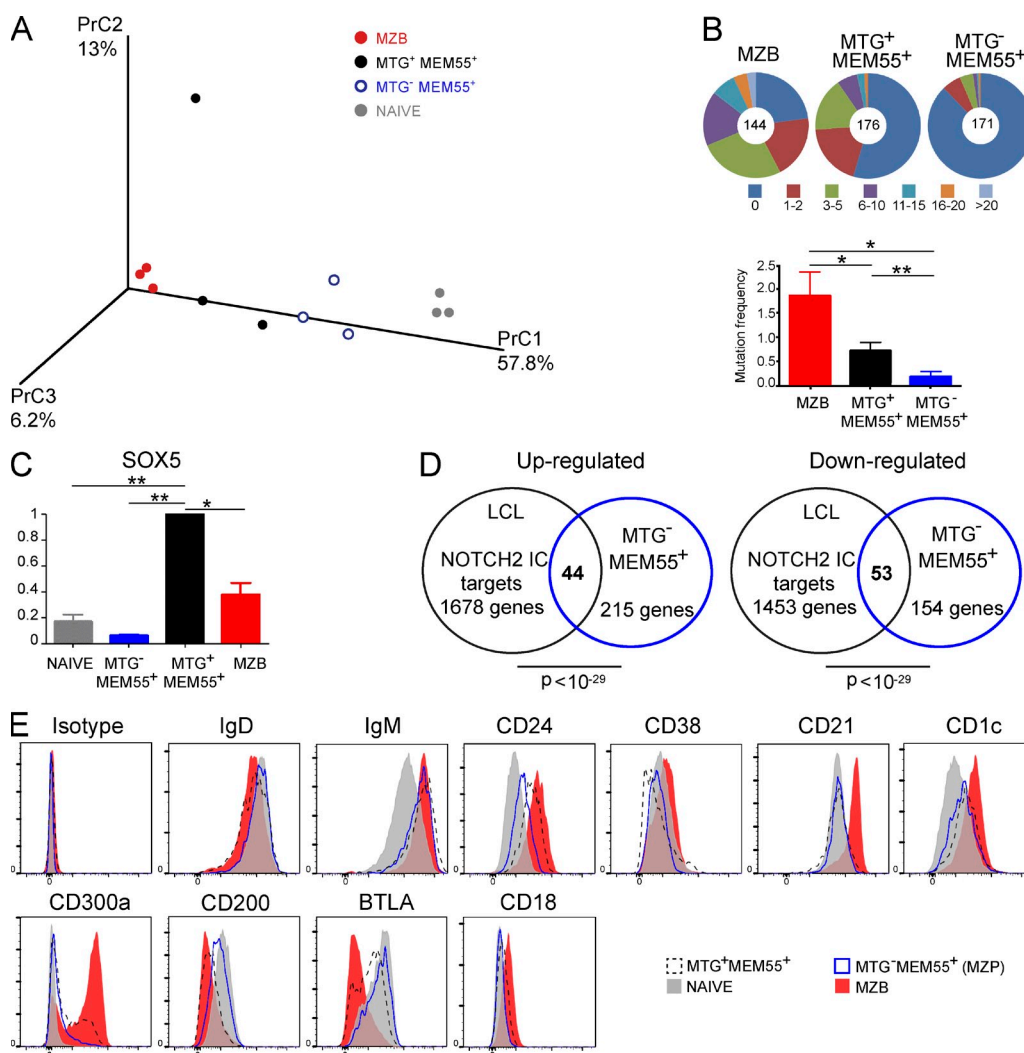


Figure 2. The MTG⁻MEM55⁺ subset represents an early MZP cell stage before Ig gene diversification. (A) Gene expression profiles of naive, MZB, MTG⁻MEM55⁺, and MTG⁺MEM55⁺ cells were determined using Affymetrix Human Genome U133 2.0 Plus microarrays (see Materials and methods). A 3D representation of a principal component analysis (PrC) performed for these four subsets, based on the expression of the 1,855 probes that were differentially expressed between naive and MZB cells, with a fold change ≥ 2 ($P < 0.05$), is shown, with each dot representing a single sample. (B) Mutation distribution within Ig sequences from splenic MZB, MTG⁺MEM55⁺, and MTG⁻MEM55⁺ subsets and mutation frequencies per total sequences. Mutations were analyzed within 284 pb of rearranged J_H4-J_H5 intronic sequences with data pooled from five children (detailed in Fig. S1). The pie charts depict relative proportions of sequences with a given mutation range (see the color legend). The total number of analyzed sequences is indicated in the center of each chart. Mutation frequencies of all sequences from each subset are represented, expressed as mutations per 100 bp (mean of 5 splenic samples \pm SEM). **, $P < 0.01$; *, $P < 0.05$; paired, two-tailed Student's *t* test. (C) Relative expression levels of *SOX5* were determined by qPCR for naive, MZB, MTG⁺MEM55⁺, and MTG⁻MEM55⁺ cells. Expression values normalized by *B2M* expression were calculated by the comparative method, normalizing to 1 the expression of the different genes in the MZB fraction. Mean values \pm SEM of three independent experiments done in triplicates are shown. **, $P < 0.01$; *, $P < 0.05$; paired, two-tailed Student's *t* test. (D) Through data mining, a list of 1,678 and 1,453 genes that were, respectively, up or down-regulated after induction of an activated NOTCH2 receptor (NOTCH2-IC) in an EBV-transformed human B lymphoblastoid cell line (LCL) was established. Those genes were compared with the 215 and 154 genes that were, respectively, over- or under-expressed in MZP compared with naive cells (with a fold change ≥ 1.5 , $P < 0.05$) to generate Venn diagrams. The numbers of genes that are common in both lists are indicated in bold at the intersection between two circles. Hypergeometric distribution was used to calculate the *p*-value according to GSEA. (E) After gating on dump⁻CD19⁺ cells, and based on their respective expression of MTG, MEM55, CD27, and IgD, naive (gray), MZB (red), MTG⁻MEM55⁺ (blue), and MTG⁺MEM55⁺ (black, dotted line) cells from children spleen samples were analyzed for expression of several surface markers by flow cytometry. Data are representative of 3 different samples.

that they may also have experienced NOTCH2-dependent activation in vivo (unpublished data).

To better characterize the phenotype of MZP cells, several cell surface markers discriminating MZB from naive B cells were analyzed by flow cytometry but, except for CD24,

CD1c, and IgM, none of the tested markers were differentially expressed between naive and MZP cells (Fig. 2 E). When compared with splenic naive and MZB cells, MZP displayed an intermediate expression of CD24 and CD1c. Their IgM expression was higher than naive cells (and similar to the one

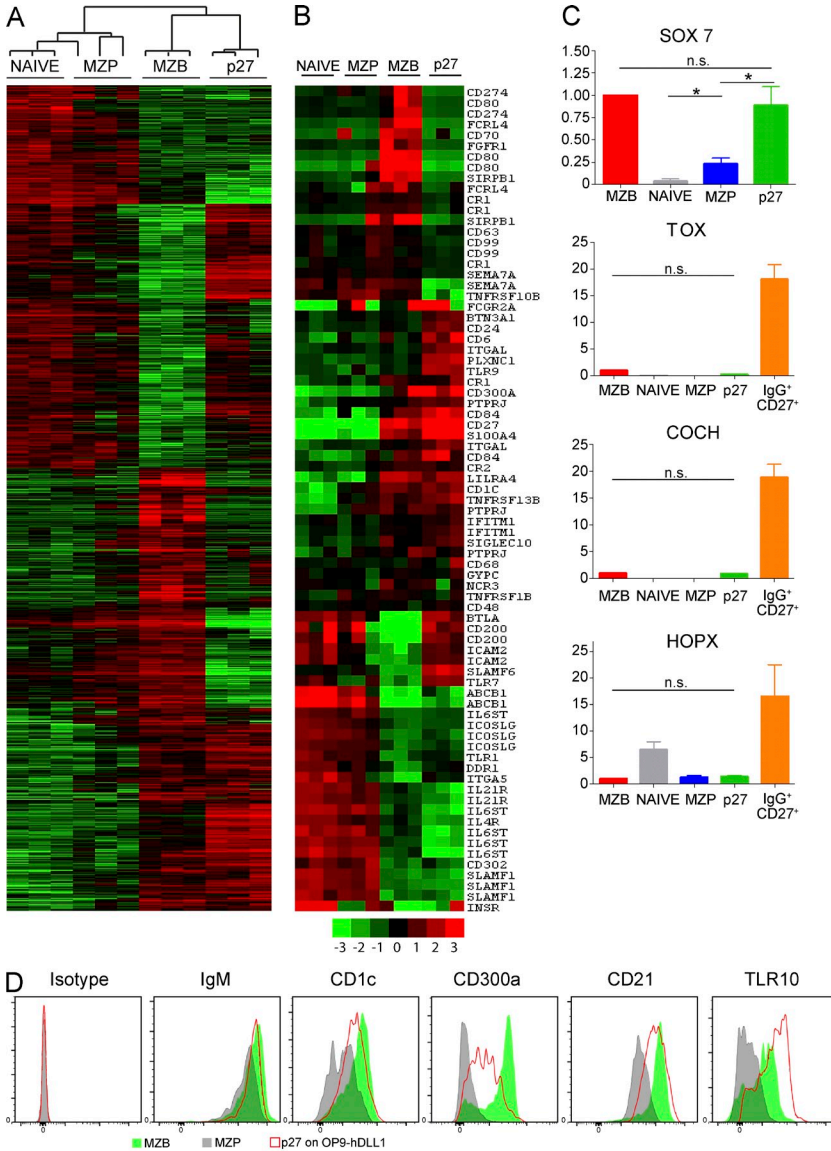


Figure 3. In vitro NOTCH2 stimulation induces MZP cells toward an MZB-like profile. (A) Ex vivo naive, MZB, and MZP (MTG⁺MEM55⁺) cells were sorted from splenic samples of 3 children as described (see Materials and methods). In parallel, after a 2-d culture on OP9-hDLL1 cells, MZP cells having acquired a CD27 expression (p27 cells) were sorted as well, and their respective gene expression profiles were determined. The array dendrogram and heatmap expression profiles of naive, MZB, MZP, and p27, obtained by hierarchical clustering using the 1,855 probes that discriminated naive from MZB cells ($P < 0.05$, twofold higher expression), are shown. Each column represents microarray data from a sample of the indicated cell subtype and each row represents the expression of a single gene. Red squares indicate increased expression and green squares indicate decreased expression relative to the median expression of the gene according to the color bar shown (\log_2 scale). (B) Among the 1,855 probes discriminating MZB from naive B cells, those corresponding to cell surface proteins using the GSEA tool were determined, and the heatmap expression profile of these surface markers are represented for each splenic sample. (C) Relative expression levels of *SOX7*, *TOX*, *COCH*, and *HOPX* (see Fig. 4) were determined by qPCR for the very fractions of naive, MZB, MZP, and p27 cells that have been used for the microarray-based gene expression analysis and for IgG⁺CD27⁺ cells from the same donors. Expression values normalized by *B2M* expression were calculated by the comparative method, normalizing to 1 the expression of the different genes in the MZB fraction. Mean values \pm SEM of three independent experiments done in triplicates are shown. No differences were observed between p27 fractions and MZB cells. *, $P < 0.05$; n.s., nonsignificant; paired, two-tailed Student's *t* test. (D) After gating on CD20⁺ cells, CD27-positive cells (p27) obtained after a 3-d culture of MZP on OP9-hDLL1 (red line) and ex vivo MZP (gray) and MZB (green) cells were analyzed for expression of several surface markers by flow cytometry, with GFP⁺ OP9 cells excluded from the analysis gate. Data are representative of 3 different samples.

of MZB cells), while they expressed high levels of IgD, like naive B cells. Conversely, the expression of CD21 was lower on MZP and naive B cells as compared with its high expression on MZB cells. Altogether, the phenotype of MZP cells is ABCB1⁺MEM55⁺CD27⁻IgM^{high}IgD^{high}CD21⁺CD1c^{int}CD24^{int}Cd38^{int}.

Transcriptional profiling of in vitro-derived MZ-like B cells

A fraction of MZP cells cultured with OP9-hDLL1 cells differentiated into CD27-expressing cells (termed p27). To determine if such cells acquired other MZ-like characteristics and to delineate their relationship with naive and MZB cells, p27 cells obtained after 2 d of culture were sorted and their gene expression profile was determined and compared with those of ex vivo-sorted naive, MZB, and MZP cells. We

performed a hierarchical clustering of the four cell fractions (each represented by three independent samples), based on the expression of the 1,855 probes used previously that discriminates MZB from naive cells with a twofold change. We found that p27 cells clustered with MZB cells in one arm of the dendrogram, while naive and MZP B cells clustered in the other arm (Fig. 3 A). Thus, after in vitro differentiation from MZP, p27 cells have acquired a gene expression profile that makes them closer to MZB for the interrogated set of genes. Among this list of 1,855 discriminating probes, we focused on the 50 cell surface markers identified according to GSEA annotation (<http://www.broadinstitute.org/gsea/index.jsp>). Their expression levels in the various samples are depicted in Fig. 3 B. Interestingly, some surface marker-coding genes associated with the MZB and/or the CD27⁺ profile

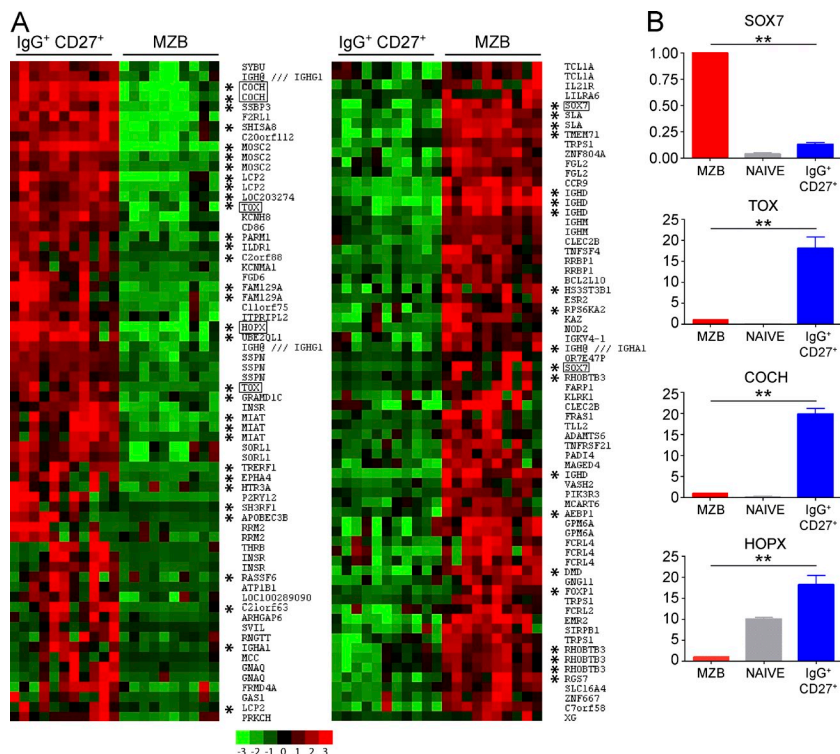


Figure 4. *TOX*, *HOPX*, *COCH*, and *SOX7* display a markedly different expression between MZB and switched B cells. (A) Splenic IgG⁺CD27⁺ and IgD⁺CD27⁺ (MZB) cells were sorted from either 10 or 11 spleen samples from donors of different ages (see Materials and methods) and their gene expression profiles were determined. The 50 genes that achieve the highest difference in expression ($P < 0.05$) between those two subsets in spleen are shown (left, up-regulated in IgG⁺CD27⁺; right, up-regulated in MZB cell; the log₂ scale bar is indicated), with spleen samples arrayed by increasing age. The same comparison was made for blood IgG⁺CD27⁺ and MZB IgD⁺CD27⁺ (not depicted) to establish a list of the 50 most discriminating genes. The discriminating genes that are shared between the blood and spleen comparisons are identified by asterisks, and the four genes studied by qPCR are boxed. (B) MZB, naive, and switched IgG⁺CD27⁺ cells from splenic samples of four different children were obtained by two consecutive sorts (see Materials and methods). Relative expression levels of *SOX7*, *TOX*, *COCH*, and *HOPX* in each subset were determined by qPCR. Expression values normalized by *B2M* expression were calculated by the comparative method, normalizing to 1 the expression of the different genes in the MZB fraction. Mean values \pm SEM of three independent experiments done in triplicates are shown. **, $P < 0.01$; paired, two-tailed Student's *t* test.

(*CD1c*, *CR2*, *TNFRSF13B*, and *TLR9*) were up-regulated in p27 cells, whereas the *ABCB1* transporter gene, as well as *IL21R* and *IL4R*, were down-regulated. At the cell surface expression level, up-regulation of *CD1c*, *CD21*, and *TLR10* was observed during in vitro culture on OP9-DLL1 cells (Fig. 3 D). Also of interest was the up-regulation in p27 of Notch target genes: *DTX1*, highly expressed in MZB, and the recently identified *CD300a* gene (Kohlhof et al., 2009; Moellering et al., 2009), expressed by mature CD27⁺ B cells in both blood (Silva et al., 2011) and spleen (microarrays deposited in the Array-Express database). In our in vitro induction, *CD300a* up-regulation by MZP was confirmed at the protein level in p27 reaching an intermediate value between MZP and MZB cells (Fig. 3 D), with addition of a NOTCH2-blocking antibody abolishing the *CD300a* induction (not depicted).

In an attempt to find diagnostic genes that not only discriminate CD27⁻ from CD27⁺ B cells but also MZB from CD27⁺IgG⁺ cells, we compared the gene expression profile of these two populations. To this end, splenic MZB and IgG⁺CD27⁺ B cells, isolated from 10 and 11 spleen samples, respectively (from 4 children between 4 and 8 yr, 3 adults, and 3–4 seniors >75 yr), were analyzed on microarrays. Starting from the genes that were differentially expressed between splenic IgG⁺CD27⁺ and MZB cells (with a fold change ≥ 2 ; $P < 0.05$), we determined the 50 most significant genes (either under- or overexpressed) that achieved the highest fold change (Fig. 4 A). 35 of them were also present among the 50 most differentially expressed genes between IgG⁺CD27⁺ and

MZB cells from blood (23 up-regulated and 12 down-regulated in switched cells, unpublished data) and are marked by an asterisk in Fig. 4 A. Among those 35 discriminating genes, we selected 4 genes of particular interest: *COCH*, *TOX*, and *HOPX*, which were >10-fold overexpressed in switched cells, and *SOX7* which was 10-fold overexpressed in MZB cells. Similar differences were also observed for these genes between splenic IgA⁺ and MZB cells (unpublished data). *TOX* and *HOPX* code for transcription factors that play a major role in various immune subsets, and notably in the transcriptional regulation of exhausted CD8 T cells for *TOX* and of T_H1 effector memory for *HOPX* (Albrecht et al., 2010; Doering et al., 2012), whereas cochlin, an extracellular matrix protein coded by the *COCH* gene, has been recently proposed to be secreted by follicular dendritic cells and to modulate immune responses (Py et al., 2013). *SOX7* is a transcription factor known to be an important player in the molecular regulation of the first committed blood precursors (Séguin et al., 2008). It is noteworthy that *SOX7* is the most discriminating transcription factor identified to be up-regulated in MZB compared with switched cells both in spleen and blood (Fig. 4 A and not depicted). These four selected genes were further validated by quantitative real-time PCR (qPCR) performed on sorted splenic MZB, naive, and switched IgG⁺CD27⁺ cells (Fig. 4 B). *SOX7* was confirmed to be ~8 \times more expressed in MZB cells than in switched cells, whereas *COCH*, *TOX*, and *HOPX* were ~20 \times more expressed in switched IgG⁺CD27⁺ cells than in MZB cells. Although *SOX7*, *TOX*,

and *COCH* had minimal expression in naive B cells, the *HOPX* expression profile was different; it was expressed at an intermediate level in naive cells, down-regulated in MZB, and up-regulated in switched B cells.

The expression of these four discriminating genes was tested in the p27 fraction and in the ex vivo–sorted MZB, naive, and MZP cells fractions used in the microarray analysis, as well as in IgG⁺CD27⁺ cells from the same donors. *SOX7* was already expressed at a low level in MZP cells but its expression increased in p27 cells to a comparable level to the one observed in MZB cells. In contrast, none of the IgG⁺CD27⁺-related diagnostic genes (*TOX*, *COCH*, and *HOPX*) were induced in p27 cells, their relative expression being similar or lower in p27 compared with MZB cells (Fig. 3 C). It is noteworthy that *HOPX*, whose expression is at an intermediate level in naive cells compared with switched cells, was also already shut down at the MZP stage and remained at a similar expression level during the differentiation from MZP to p27 cells. In conclusion, for the interrogated set of genes that discriminates MZB from naive CD27⁻ cells, in vitro–differentiated p27 cells showed a gene expression profile closer to the one of MZB cells and, most strikingly, acquired or maintained the MZB pattern of expression for the four diagnostic genes that distinguish MZB from other CD27⁺ subsets.

Age-related decline of the MZP B cell subset

We next wanted to determine the frequency of MZP among CD19⁺ B cells in the spleen as a function of age and therefore analyzed a cohort of donors from various ages (15 children: 4–9 yr old, and 24 adults: 10–78 yr old). We observed a mean frequency of $4.4 \pm 0.44\%$ in the spleen of children under 10 yr of age, whereas the mean frequency dropped to $1.7 \pm 0.26\%$ in older individuals, this difference being highly significant (Fig. 5 A). MZPs were also found in the blood (25 children: 1–9 yr old, and 10 adults) at a mean frequency of $6.7 \pm 0.16\%$ at <10 yr of age. As for spleen, MZPs in blood were present at a lower frequency (a mean of $1.9 \pm 0.27\%$) in older individuals.

In conclusion, MZP cells are more frequent in young individuals but are nevertheless present throughout life, being

possibly able to replenish the MZB cell pool. We studied also the frequency of MTG⁺MEM55⁺ cells, which correspond to more mature cells (Fig. 5 B). Their frequency shows minor variation with age in the spleen, staying around 4%. A slight decrease with age was observed in the blood, with a mean frequency of 4.4 ± 0.4 (SEM) at <10 yr of age and 2.6 ± 0.3 in older individuals.

DLL1-expressing cells are present in the human splenic MZ

It has been proposed that MZP cells in the mouse encounter the Dll1 ligand on fenestrated venules in the MZ and at its periphery (Tan et al., 2009). To localize DLL1-expressing cells in the human spleen, splenic cryosections from children (aged from 2 to 6 yr) were stained for DLL1, together with IgD and CD27 (which allow the identification of splenic lymphoid structures), and examined by confocal microscopy (Fig. 6). The sections contained generally numerous secondary B cell follicles, one of these full-blown IgD-negative GCs surrounded by an IgD-positive zone shown in Fig. 6 A. Two distinct areas within the IgD⁺ zone are visible, an inner zone of CD27-negative IgD⁺ cells corresponding to the corona (Co) and mostly populated by naive B cells, and an outer zone corresponding to the MZ with CD27⁺ cells that express IgD at lower level. Some CD27^{high} cells, most probably T cells but also possibly plasma cells and/or memory B cells, are also scattered in the MZ. At one pole of the follicle, a CD27^{high} zone that did not stain for IgD corresponds to the periarteriolar lymphatic T cell sheath (PALS) that surrounds an arteriole. Although a DLL1 staining is visible on this arteriole, only very few DLL1-expressing cells were seen in the red pulp and none in the corona. In contrast, DLL1⁺ cells that did not stain for IgD or CD27 were clearly present in the MZ of all the children's spleen samples that were analyzed; however, their numbers were variable from one sample to another (Fig. 6, B and C, showing different DLL1⁺ cell densities). These DLL1⁺ cells were of elongated and irregular shape, suggesting a nonlymphoid nature, and were intermingled with lymphoid cells. Interestingly, some IgD^{high}CD27⁻ cells scattered in the MZ were in close vicinity with DLL1⁺ cells (Fig. 6 C, i and ii, enlarged insets).

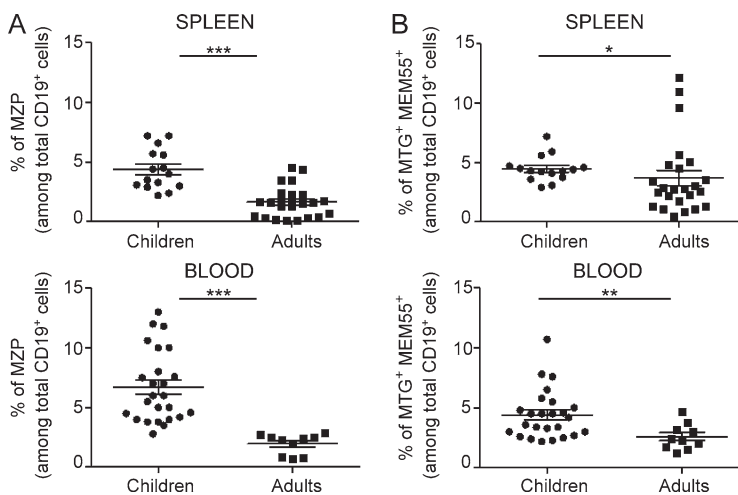


Figure 5. Splenic MZP frequencies decline with age in spleen and blood. (A) Frequencies (expressed as percentages of total CD19⁺ B cells) of Dump⁻CD19⁺-gated IgD⁺CD27⁻MTG⁻MEM55⁺ (MZP) cells in spleen (top) and blood (bottom) from children and adults. (B) The same analysis performed for MTG⁺MEM55⁺ cells in spleen (top) and blood (bottom) for children and adults. Age range for children's spleen samples: 4–9 yr; for blood samples: 1–9 yr. Mean values \pm SEM are indicated on the graphs. ***, $P < 0.001$; **, $P < 0.01$; *, $P < 0.05$; Mann-Whitney statistical test.

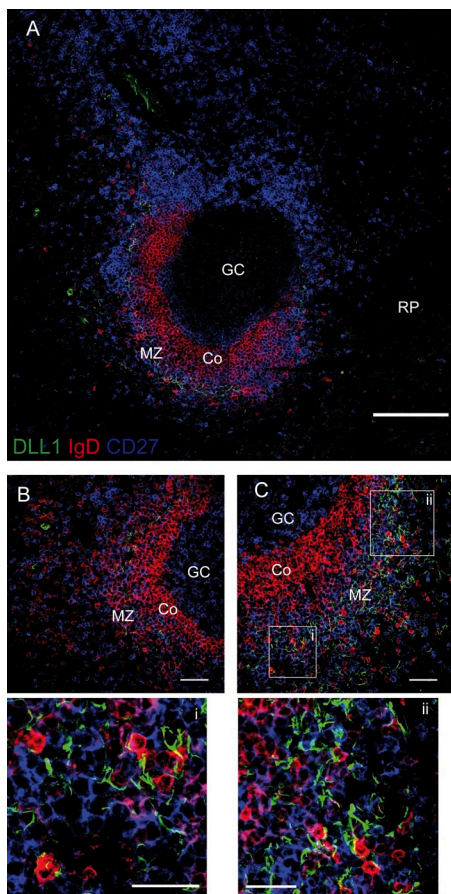


Figure 6. Non-lymphoid DLL1⁺ cells are located in the splenic MZ. Confocal imaging analysis of spleen sections from children stained with fluorescence-conjugated anti-DLL1 (green), anti-IgD (red), and anti-CD27 (blue; original objective lens magnification 40 \times). (A) One representative image (out of three splenic samples analyzed) of a GC surrounded by densely distributed IgD⁺CD27⁻ naive cells forming the corona and the MZ at the periphery, occupied by CD27⁺IgD^{low} B cells (lightly colored in purple; splenic section of a 4-yr-old child; bar, 150 μ m). (B and C) Selected areas of splenic sections (from 2- and 4-yr-old children, respectively), illustrating the presence at various density of DLL1⁺ cells in the MZ. Note the complete absence of DLL1 staining in the corona (bars, 50 μ m). The insets i and ii show, respectively, a four- and threefold magnification of DLL1-positive cells that are in close contact with IgD^{high} cells in the MZ (bars, 30 μ m). Co, corona; RP, red pulp.

However, it was not possible to establish if these cells were bona fide MZP cells rather than transitional B cells, given the absence of a reliable staining allowing the unequivocal identification of such cells on cryosections. In conclusion, the NOTCH2 engagement on immature B cells, including MZP, may take place in the MZ itself via interaction with DLL1⁺ nonlymphoid cells.

Patients heterozygous for a Notch2 mutation (Alagille syndrome) display a marked reduction of their blood MZB cells
In the spleen of mice with B cell-restricted Notch2 deficiency, MZB cells are virtually absent. Furthermore *Notch2*

haploinsufficiency in the B cell lineage compromises MZB cell differentiation, with the numbers of MZB cells ranging from one sixth to one fourth of those in control mice (Saito et al., 2003). To evaluate the incidence of a NOTCH2 deficiency on the development of MZB cells in humans, we searched for a condition where NOTCH2 mutations have been described. This is the case for the Alagille syndrome (ALGS), a rare (1:70,000) autosomal dominant disorder with variable multisystem organ involvement, which is caused by mutations in one of two genes in the Notch signaling pathway, *JAG1* (a Notch ligand) or *NOTCH2*. The majority of cases (~94%) are caused by haploinsufficiency of the *JAG1* gene, and a small percentage of cases are caused by heterozygous mutations in *NOTCH2*. We could have access to blood samples from four patients (7, 8, 10, and 32 yr old) who presented an Alagille syndrome with NOTCH2 mutations (Fig. 7 A). Thus, to evaluate whether the development of MZB cells was altered in these four patients, peripheral blood B cell subsets were analyzed by flow cytometry after CD19, IgD, and CD27 staining (Fig. 7, B and C; and Table S2). In healthy controls, the frequency of MZB and switched B cells may vary widely while staying at a similar frequency for each individual, i.e., displaying an MZB to switched cell ratio of one (Fig. 7 D). In the four Alagille patients, the proportion of MZB (IgD⁺CD27⁺) cells was low compared with age-matched controls, but more strikingly, the MZB to switched cells ratio was reduced (2.3-fold on average). The two MTG⁻/MTG⁺MEM55⁺ subsets were analyzed for the adult patient and were within the normal, adult range, whereas the residual MZB subset showed CD1c expression comparable to healthy controls (unpublished data). Three Alagille patients presenting with a *JAG1* mutation were also studied: one child (11 yr old) had low overall CD27⁺ B cell numbers, whereas the other two (3 and 4 yr old) had normal IgD⁺CD27⁺ B cell frequencies for their age (Table S2), which indicated that reduction in the MZB subset in Alagille patients is more specifically associated with a deficiency in the Notch2 signaling pathway. Although one cannot exclude that the reduced frequency of MZB cells observed in the NOTCH2 heterozygous patients may come from a compromised survival that would be restricted to this subset, the similar phenotype induced by Notch2 insufficiency in mice and humans strongly argues in favor of a similar NOTCH2-dependent commitment of human MZB cells.

DISCUSSION

Notch2 interaction with its ligand, Dll1, is required in the mouse to drive MZP into the MZB cell lineage (Saito et al., 2003; Hozumi et al., 2004). Preliminary data based on humanized mouse models have also proposed a Notch2 dependence for the differentiation of IgM⁺IgD⁺CD27⁺ B cells (Scheeren et al., 2008). Accordingly, we searched for an MZP in the spleen from young children, taking as diagnostic criteria its capacity to acquire an MZ phenotype when cultured in presence of OP9 cells expressing human DLL1, a differentiation which, moreover, should be specifically inhibited in presence

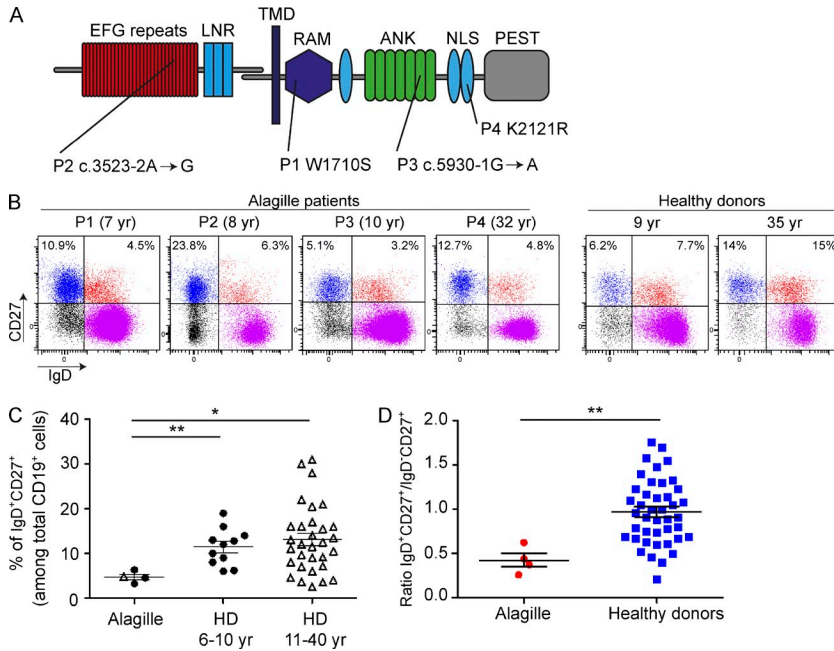


Figure 7. NOTCH2 haploinsufficiency results in a reduced proportion of circulating MZB cells. (A) Scheme of the NOTCH2 protein with its different domains. The extracellular domain of NOTCH2 contains 36 epidermal growth factor (EGF) repeats involved in ligand binding and three Lin/Notch repeats (LNRs). The intracellular portion of the protein includes seven ankyrin repeats (ANK) required for binding and activating the RBPJ transcription factor, flanked by nuclear localization signals (NLSs). Other domains include: a transmembrane domain (TMD), an RBP-J-associated module (RAM), and a proline/ glutamic acid/serine/threonine rich domain (PEST) involved in proteosomal degradation. The mutations identified in the four Alagille patients studied are depicted; two affect splicing sites at intron borders (P2 and P3) and two are a missense mutation in RAM domain (P1) or NLS (P4). (B) Blood B cells from four patients heterozygous for NOTCH2 mutations and age-matched controls (healthy donors, HDs) were analyzed by flow cytometry after IgD, CD27, and CD19 staining. The proportion of IgD⁺CD27⁺ (MZB) and switched IgD⁻CD27⁺ (as a percentage of total B cells) for each of them is indicated on dot plots.

(C) Relative frequencies of blood IgD⁺CD27⁺ cells (expressed as percentages of CD19⁺ B cells) of Alagille patients (three children and one adult, same symbols as for age-matched control group) and healthy donors (HDs) that were divided into two age groups as indicated. (D) Ratios of IgD⁺CD27⁺ versus switched cells were plotted for each patient and for a control group (with ages varying from 6 to 40 yr), with mean values ± SEM indicated by error bars. **, P < 0.01; *, P < 0.05; Mann-Whitney statistical test.

of anti-NOTCH2 blocking antibodies. This precursor subset was identified using the recently described MEM55 antibody, which marks a glycosylated variant of the CD45RB molecule, harbored by CD27⁺ B cells and an immature B cell subset (Koethe et al., 2011). Surprisingly, these MZPs were further characterized as expressing the ABCB1 transporter reported so far as the unique hallmark of naive B cells (Wirhth and Lanzavecchia, 2005) and harbored an IgM^{high}IgD^{high}CD27⁻CD24^{int}CD38^{int}ABCB1⁺MEM55⁺CD21⁺CD1c^{int} surface phenotype. At the transcriptional level, MZPs were closer to naive than to MZB cells (a difference of 249 gene probes compared with naive vs. 990 with MZB, considering a two-fold change and a p-value < 0.05) and accordingly carried an unmutated BCR for most of them. Interestingly, comparison with a transformed human B cell line induced to express an activated NOTCH2 receptor (Kohlhof et al., 2009) revealed that MZPs were already partly engaged in the NOTCH2 pathway, most probably through inductive cues that they encountered upon their splenic location.

Upon in vitro induction by DLL1, their transcriptional profile became closer to MZB, with the up-regulation of classical MZB cell markers such as CD1c, DTX1, and CR2 (CD21). Other markers induced, like CD27, CD300A, or TNFSFR13B (TACI) discriminate all CD27⁺ subsets from naive B cells but are not specific for MZB cells. Switched and IgM⁺IgD⁺CD27⁺ cells have indeed been shown to share many transcriptional similarities (Good et al., 2009). However, we performed a transcriptional analysis of 12 spleen samples from various ages (children, adult, and senior) to identify diagnostic

genes that would be differentially expressed by these two populations. Four genes were selected that constitute a specific signature of MZB cells, presenting a >10-fold expression difference with switched memory B cells, a difference which was also observed between blood subsets (unpublished data): SOX7, TOX, COCH (Cochlin), and HOPX. SOX7 was found to be highly expressed in blood and splenic MZB cells while being at a low level in IgG⁺ and IgA⁺CD27⁺ B cells, but it was not differentially expressed by mouse MZB cells (our unpublished data). SOX7 is a member of the Sox family of transcription factors, which has been involved in several developmental processes as well as in the maintenance of self-renewal and multipotent capacity in stem cells and progenitor cells (Séguin et al., 2008). Conversely, TOX, COCH, and HOPX were highly expressed in splenic and blood switched B cells, as opposed to their low expression in MZB cells. Among them, only Tox was more highly expressed by mouse memory B cells (ImmGen database). These three genes have recently emerged as new players in the immune system: for Hoxp as a lineage-commitment transcription factor (Albrecht et al., 2010), for Tox as a transcription network nodal point (Doering et al., 2012), and for Coch—which had been mainly known for being mutated in a human deafness congenital disease—as an immune response adjuvant secreted by follicular dendritic cells (Py et al., 2013). However, their role in the generation and maintenance of switched memory B cells in humans is unknown at the moment. Remarkably, SOX7, already expressed at a low level in MZP, was induced up to its MZB level during the in vitro induction process (fourfold).

This transcription factor may thus come out as a major regulator for this differentiation pathway in humans, although we do not know at this stage which gene expression it controls. Conversely, *TOX*, *HOPX*, and *COCH* remained at a low level during in vitro induction, strongly supporting the proposition that this induction was specifically driving MZP B cells toward the MZB cell lineage and not broadly inducing a CD27-like activated profile.

Interestingly, the immature B cell fraction originally described by Koethe et al. (2011), which did not express the *ABCB1* gene, was also inducible in the in vitro induction assay using the up-regulation of CD27 as a read-out. However this induction was already very potent in the absence of DLL1 with the OP9 stroma, and it was not significantly inhibited by the addition of an anti-NOTCH2 blocking antibody. Moreover, >50% of these cells carried somatic mutations on their BCR. This *ABCB1*⁻*MEM55*⁺ B cell fraction, which, as opposed to MZP, appears closer at the transcriptomic level to MZB than to naive B cells, could therefore represent a more advanced stage of differentiation toward the MZB lineage. In contrast, this *ABCB1*⁻*MEM55*⁺ population differs from all other splenic subsets by its expression of *SOX5*, another member of the Sox family. *SOX5* expression has been reported in tissue-based memory B cells, described as a CD27⁻ subset in tonsils and related to exhausted B cells identified in the blood of HIV-infected patients (Ehrhardt et al., 2008; Moir et al., 2008). *SOX5* expression was also reported in anergic B cells, although this later subset is CD27⁺ (Charles et al., 2011). Whether *ABCB1*⁻*MEM55*⁺ B cells represent a diverted MZ maturation stage rather than an advanced MZ precursor is obviously an open issue that warrants further study.

Many questions obviously remain concerning MZP B cells. Where, in a linear model of differentiation, should they be placed, since they carry immature and naive B cell markers at the same time? What is their contribution throughout life toward the MZB lineage, assuming that splenic MZB cells should be replaced as they are engaged in immune responses? Consistent with this, although their frequency declines with age, MZPs were still present in the spleen and blood of adults. Moreover, confocal analysis of splenic sections revealed that DLL1 is expressed, as in the mouse, on an intricate network of nonlymphoid cells within the MZ in young children. Interestingly, B cell depletion studies have reported that reemergence of MZB cells may lag behind switched cells, suggesting that precursors, inducing cells, or factors may be more limiting in the adult (Roll et al., 2006).

MZB cell lymphomas are neoplasms of mature B cells, a subset of which are localized in the splenic MZ. Exome sequencing showed that mutations in the *NOTCH2* pathway were present in 30% of these tumors with, in many instances, a mutation in the C-terminal PEST domain of NOTCH2 that controls its proteosomal degradation (Kiel et al., 2012; Rossi et al., 2012). Because a constitutive activation of NOTCH2 was associated with a splenic MZB cell malignant phenotype and not with any other type of B cell lymphoma, it was instructive to find out whether NOTCH2 insufficiency would

conversely disclose a MZB cell phenotype. The Alagille syndrome is a multisystem autosomal dominant genetic disorder that affects the liver, the heart, and the eyes, along with skeletal abnormalities and facial features (Kamath et al., 2012). Microdeletions of the *JAG1* gene that disrupt the NOTCH2 pathway are usually associated with this syndrome, but in rare cases in which *JAG1* is not mutated, patients present an inactivating mutation on one of their *NOTCH2* allele. Strikingly, and as observed for mouse splenic MZB cells with a heterozygous *Notch2* inactivation, analysis of blood B cells from NOTCH2 haploinsufficient Alagille patients showed a reduction of their IgD⁺IgM⁺CD27⁺ cells, while their switched B cells were at a normal level.

The existence of a human blood and splenic MZB cell subset was put into question, notably through the work of Seifert and Küppers (2009), who reported that CD27⁺ blood B cells originated for most of them from a GC precursor cell, which gave rise to both IgM⁺ and switched B cells. Surprisingly, these data were challenged by recent studies involving high throughput sequencing of the different blood B cell subpopulations from several healthy donors, which did not reveal any clonal relationship between blood IgD⁺IgM⁺CD27⁺ and switched cells. In contrast, such relationships could be found between other B cell subsets, like CD27⁺ and CD27⁻ switched or IgM-only cells or, even more rarely, between IgD⁺IgM⁺CD27⁺ and IgM-only B cells (Wu et al., 2010b, 2011). Further studies using high throughput sequencing of paired blood and spleen samples may help to decipher further clonal relationships between B cell subsets and clarify this issue. Altogether, the NOTCH2 dependence observed in Alagille patients for the development of the IgM⁺IgD⁺CD27⁺ MZB cell subset, along with the identification of a candidate splenic MZB cell precursor reported here, brings new evidence in favor of the existence of a separate MZB cell lineage in humans.

MATERIALS AND METHODS

Samples and mononuclear cell isolation. This study was conducted in accordance with the Declaration of Helsinki, with informed consent obtained from each patient or the patient's family. Spleen and blood samples were obtained from children undergoing a splenectomy for nonimmunological disease-related reasons (spherocytosis or drepanocytosis). Leftover blood samples (taken for blood counts) from healthy children undergoing orthopedic surgery were obtained from the Service d'Hématologie Biologique of the Necker Hospital. Adult spleen and blood samples were obtained, respectively, from organ donors with the authorization of the French Agence de la Biomédecine and from the blood bank (Etablissement Français du Sang). Alagille patients with Notch2 heterozygous mutations were diagnosed by the French Reference Center for the molecular diagnosis of Alagille syndrome (A. Guiochon-Mantel). Spleen MNCs and peripheral blood mononuclear cells were obtained, respectively, from mechanically disrupted spleen samples and heparinized blood after a density gradient centrifugation on Ficoll-Paque PLUS (GE Healthcare).

ABCB1 transporter activity assay. Because available specific anti-ABCB1 mAbs give only poor stainings, the expression of the ABCB1 transporter is usually detected by measuring the extrusion of MTG FM (Wirths and Lanzavecchia, 2005; Palanichamy et al., 2009). Thus, to distinguish ABCB1-positive from -negative cells, cells were diluted at 10⁷ cells/ml in RPMI (Gibco) and pulsed at 37°C under 5% CO₂ with MTG (Molecular Probes) at 20 nM for 30 min. After three washes, cells were chased for 1 h at 37°C under

5% CO₂ and were then stained on ice with additional Abs before flow cytometry analysis. Cells that do not express the ABCB1 transporter fully retain MTG, whereas ABCB1⁺ cells are MTG⁻.

Flow cytometry analysis and cell sorting. All the immunofluorescence stainings were performed by incubating cells with antibodies (described in Table S2) in PBS with 2% FCS on ice for 15 min. After a final wash, labeled cells were briefly incubated with the Sytox blue Dead Cell stain (Life Technologies), allowing the exclusion of dead cells in all the subsequent flow cytometric data acquisitions and cell sorts which were performed, respectively with a FACSCanto II and FACSAria Cell Sorter (BD). Data were analyzed either with Diva (BD) or FlowJo (Tree Star) software. The distinct cell fractions analyzed in the present work were isolated through purification, staining, and sorting procedures that vary depending on experiments and that are detailed hereafter. Both for the *in vitro* differentiation assays and microarray analysis shown in Figs. 1, 2, and 3, CD27⁻ cells were first enriched from total spleen MNC by negative selection with the EASYSEP Human naive B cell Enrichment kit (STEMCELL Technologies), which removes unwanted cells with mouse IgG1 antibodies recognizing CD27 and non-B cell markers. Thus, to avoid any possible residual contamination with CD27⁺ B cells, after the pulse/chase step with MTG, the enriched CD27⁻ cells were further incubated with a biotin rat anti-mouse IgG1. After a wash, cells were first incubated with saturating concentrations of 100 µg/ml mouse IgG1 for 15 min on ice before adding a combination of anti-CD24, -CD38, -IgG, -IgA, -IgE, -CD27, -CD20, -CDR45RB (MEM55 clone) antibodies for an additional 15-min incubation time. After a final wash, cells were incubated with a streptavidin conjugate, allowing us to further exclude the remaining rare CD27⁺ cells from the sorting gates. Both for the differentiation assay and microarray analysis, four distinct CD20⁺IgG⁻IgA⁻IgE⁻CD27⁻ fractions were sorted based on their MTG and MEM55 expression: transitional (MTG⁺MEM55⁻) cells, naive (MTG⁻MEM55⁻) cells, MTG⁻MEM55⁺ (also designed as MZP in Fig. 3) cells, and MTG⁺MEM55⁺ cells. CD24/CD38 expression of these different subsets, along with sorting gates, is indicated in Fig. 1.

The cells designed as MZB (Fig. 2 A; and Fig. 3, A–C) and IgG⁺CD27⁺ (Fig. 3 C) were isolated as follows. Total splenic MNC pulse/chase with MTG, labeled with a combination of anti-CD3, -CD14, -CD16, -CD24, -CD38, -IgD, -IgG, -CD27, and -CD20 antibodies, were sorted with gates set on CD3⁺CD14⁻CD16⁻ (dump⁻) CD20⁺CD27⁺CD24⁺CD38^{low} cells that were further divided into IgG⁺IgD⁺ (MZB) or IgG⁺IgD⁻ (IgG⁺CD27⁺) fractions. The p27 fraction (Fig. 3) corresponds to MZP cells having acquired the expression of CD27 after a 2-d culture on OP9-hDLL1 cells and were sorted with gates set on IgD⁺CD20⁺CD27⁺ cells, with OP9-GFP⁺ DLL1⁺ cells excluded. Cells depicted as MZB and IgG⁺CD27⁺ in the transcriptomic analysis shown in Fig. 4 A were isolated as follows from splenic samples of 4 children (from 4 to 6 yr of age), 3 adults, and 3 (or 4) seniors of >75 yr. B cells enriched from splenic MNC with the Dynabeads Untouched Human B Cells kit (Life Technologies) were labeled either with anti-IgD, -IgM, -CD24, -CD38, -CD19, and -CD27 antibodies, or with anti-IgG, -IgA, -CD38, -CD27, and -CD19 antibodies. MZB cells (CD19⁺IgM⁺IgD⁺CD27⁺CD24⁺CD38^{low}) and CD27⁺IgG⁺ cells (CD19⁺IgG⁺IgA⁻CD24⁺CD38^{low}) were then sorted. All the fractions that were analyzed on microarrays were purified by two successive rounds of cell sorting to achieve >99% purity.

MZB, naive, and IgG⁺CD27⁺ cells in Fig. 4 B (qPCR) were isolated as follows. Total splenic MNCs were labeled with a combination of anti-CD3, -CD14, -CD16, -CD24, -CD38, -IgD, -IgG, -CD27, and -CD19 antibodies. After gating on dump⁻CD19⁺ cells, IgD⁺CD27⁺CD24⁺CD38^{low}IgG⁻ (MZB), IgD⁺CD27⁻CD24⁺CD38^{low/+}IgG⁻ (naive), and IgG⁺CD27⁺CD24⁺CD38^{low}IgD⁻ (IgG⁺CD27⁺) were purified by two consecutive sorts.

For the analysis of somatic mutations (Fig. 2 B), total splenic MNC cells were pulse/chase with MTG, labeled with a combination of anti-CD3, -CD14, -CD16, -IgD, -CD27, -CD19, and MEM55 antibodies, and after gating on dump⁻CD19⁺ cells, cells designed as MZB (IgD⁺CD27⁺), MTG⁺MEM55⁺ (IgD⁺CD27⁻MTG⁺MEM55⁺), and MTG⁻MEM55⁺ (IgD⁺CD27⁻MTG⁻MEM55⁺) were sorted.

In vitro cell differentiation assay. The differentiation potential of transitional, naive, MTG⁻MEM55⁺, and MTG⁺MEM55⁺ subsets (Fig. 1 C) was tested by plating them on mouse OP9 stromal cells engineered to express either the GFP alone (OP9) or GFP and the human Notch ligand Delta-like1 gene (OP9-hDLL1; a gift from E. Six, Institut Imagine, Paris, France; Six et al., 2007). The day before, OP9 and OP9-hDLL1 cells were plated in 48-well plates at 20,000 cells/well in MEMα medium (Invitrogen) containing 20% FCS and 1% Pen-Strep (Invitrogen). On day 0, the different subsets were sorted and collected into MEMα + 20% FCS. Each fraction was put in culture on OP9 or OP9-hDLL1 (~50,000 cells per well). For MTG⁻MEM55⁺ and MTG⁺MEM55⁺ cells, the effect of a selective blocking of the Notch2 or Notch1 signaling pathway on their differentiation was evaluated by adding an anti-NOTCH2 mAb or anti-NOTCH1 mAb at 5 µg/ml (a gift from C.W. Siebel, Genentech, South San Francisco, CA; Wu et al., 2010a) when plating the cells on OP9-hDLL1 stromal cells. On day 3, cells were removed from culture, washed, labeled with anti-CD20, -IgD, and -CD27 antibodies, and lymphoid CD20⁺GFP⁻ cells were analyzed by flow cytometry for the expression of CD27.

Microarray analysis. Total RNA was isolated from the different cell fractions using the RNeasy Micro kit (QIAGEN). RNA quality and concentration were assessed using RNA6000 Pico LabChips with a 2100 Bioanalyzer (Agilent Technologies). For the microarray analysis shown in Fig. 3, 8 ng of total RNA (corresponding to ~6,000–18,000 cells depending on the RNA content of the fractions) was preamplified by Ribo-SPIA (Ribo-single primer isothermal amplification) RNA Amplification using the Ovation Pico WTA System V2 kit (NuGEN Technologies), fragmented, and labeled with biotin using the Encore Biotin Module (NuGEN Technologies), as recommended by the manufacturer. For the microarray analysis shown in Fig. 4 A, 100 ng of total RNA (corresponding to ~140,000 cells) was amplified with the GeneChip Two-Cycle Target Labeling kit (Affymetrix). Transcript expression levels were assessed with Affymetrix human Genome U133Plus2 arrays according to the manufacturer's instruction. Fluorescence data were imported into Affymetrix Expression Console and R Bioconductor analysis software. Gene expression levels were calculated using GCRMA and flags were computed using MAS5 within R. To limit potentially biased measurements (background or saturating), all probes whose flags were absent or marginal were flagged as 0, whereas those present were flagged as 1. The group comparisons were done using a Student's *t* test. To estimate the false discovery rate, we filtered the resulting *p*-values at 0.05 and considered data with 1.5- or 2-fold changes between samples. Microarray data are available in the ArrayExpress database (www.ebi.ac.uk/arrayexpress) under accession nos. E-MTAB-2246 and E-MTAB-2244.

Confocal microscopy. Immediately after splenectomy, pieces of splenic tissue were excised and embedded in OCT (Sakura), snap frozen in liquid nitrogen, and stored at -80°C. Cryosections (7–9 µm) were cut, fixed in cold (-20°C) acetone for 15 min, rehydrated in wash buffer (TBS, pH 7.6), and incubated in blocking buffer (0.5% BSA and 10% goat serum in PBS) for 30 min at room temperature (RT). Sections were then incubated for 60 min at RT or 4°C overnight, with the indicated primary antibodies (Table S2) in the blocking buffer solution. Incubations without primary antibodies were used as control. Sections were washed three times and incubated with the secondary antibody as indicated (30 min, RT). Sections were washed and mounted in Fluoromont-G (SouthernBiotech). Images were acquired by confocal microscopy with an SP5 (Leica). Fluorescence of single channels was measured, and control reference was systematically done. Pictures were taken with a 40× objective. Images were analyzed and processed with ImageJ (version 1.46; National Institutes of Health).

Analysis of mutation frequencies in J_H4-J_H5 intron flanking rearranged V_HDJ_H4. Starting from 20,000–40,000 highly purified sorted cells, total genomic DNA was extracted with Micro DNeasy kit (QIAGEN). The J_H4-J_H5 intronic region was amplified with Phusion DNA polymerase (Finnzymes) by the use of a mixture of six FR3 primers (FR3-mix) designed

to amplify all V_H gene sequences and a primer binding 5' to the J_H5 exon, as previously described (Weller et al., 2008). PCR conditions were as follows: 40 cycles of 98°C for 10 s, 60°C for 20 s, and 72°C for 20 s. The resulting J_H4 - J_H5 PCR products were gel purified and cloned with Zero Blunt PCR Cloning kit (Invitrogen). Sequences were run in an ABI PRISM 3100 Genetic Analyzer (Applied Biosystems). Mutation frequencies were calculated by comparing the sequences obtained with germline intronic J_H4 - J_H5 sequences over 284 bp, starting at the 3' border of the J_H4 gene segment.

mRNA isolation and real-time quantitative PCR (qPCR). Total RNA was isolated from each sorted cell fraction with the RNeasy Micro kit and reverse transcribed by random priming with the AffinityScript Multiple Temperature cDNA Synthesis kit (Agilent Technologies). qPCR for the human *B2M*, *SOX7*, *SOX5*, *TOX*, *COCH*, and *HOPX* transcripts was performed with specific TaqMan gene expression assays (B2M Hs00984230_m1; TOX Hs01055573_m1; HOPX Hs041888695_m1; COCH Hs00187937_m1; SOX7 Hs00846731_s1; and SOX5 Hs00753050_51; all designed by Applied Biosystems) on a 7500 Fast Real-Time PCR System (Applied Biosystems) with the 9600 Emulation run mode. Normalized values for gene expression were determined using *B2M* as internal gene reference. PCRs with a threshold cycle (C_t) >36 were considered NS.

Online supplemental material. Fig. S1 shows mutation distribution in Ig genes of children's splenic MZB, MTG⁺MEM55⁺, and MTG⁻MEM55⁺ subsets for the five analyzed samples. Table S1 shows the percentages of different CD20⁺IgD⁺ cell subsets becoming CD27⁺ after 3 d in different co-culture conditions. Table S2 shows the percentages of CD27⁺ B cell subsets in Alagille patients and control donors. Table S3 depicts the antibodies and reagents used in flow cytometry and confocal microscopy. Online supplemental material is available at <http://www.jem.org/cgi/content/full/jem.20132203/DC1>.

We are grateful to Pr. Jean-Pierre Grunfeld for his contribution, the patients, and their families. We thank Paolo Conti, Francesca Conti, Erika Della Mina, and Remi Fritzen for their contribution. We thank Emmanuelle Six for the gift of GFP- and hDDL1-expressing vectors, and Dr. C.W. Siebel (Genentech) for the gift of anti-NOTCH1 and -NOTCH2 antibodies. We thank Lucie Da Silva for organizing and handling the collection of human spleen samples. We thank for expert training Nicolas Goudin for confocal microscopy and Jérôme Mégret for cell sorting (confocal microscopy and cell sorting facilities of Structure Fédérative de Recherche Necker).

The team "Développement du système immunitaire", INSERM U1151 is supported by the Ligue Nationale contre le Cancer ("Equipe labellisée"), the Fondation Princesse Grace, the INCA for the LYMPH-IMM-MARGE project, and by an ERC advanced investigator grant. M. Descatoire was supported by a fellowship from the Fondation pour la Recherche Médicale for the fourth year of the PhD.

The authors declare no competing financial interests.

Submitted: 21 October 2013

Accepted: 18 March 2014

REFERENCES

- Albrecht, I., U. Niesner, M. Janke, A. Menning, C. Loddenkemper, A.A. Kühl, I. Lepenies, M.H. Lexberg, K. Westendorf, K. Hradilkova, et al. 2010. Persistence of effector memory Th1 cells is regulated by Hopx. *Eur. J. Immunol.* 40:2993–3006. <http://dx.doi.org/10.1002/eji.201040936>
- Bemark, M., J. Holmqvist, J. Abrahamsson, and K. Mellgren. 2012. Translational mini-review series on B cell subsets in disease. Reconstitution after haematopoietic stem cell transplantation – revelation of B cell developmental pathways and lineage phenotypes. *Clin. Exp. Immunol.* 167:15–25. <http://dx.doi.org/10.1111/j.1365-2249.2011.04469.x>
- Charles, E.D., C. Brunetti, S. Marukian, K.D. Ritola, A.H. Talal, K. Marks, I.M. Jacobson, C.M. Rice, and L.B. Dustin. 2011. Clonal B cells in patients with hepatitis C virus-associated mixed cryoglobulinemia contain an expanded anergic CD21low B-cell subset. *Blood.* 117:5425–5437. <http://dx.doi.org/10.1182/blood-2010-10-312942>
- Cuss, A.K., D.T. Avery, J.L. Cannons, L.J. Yu, K.E. Nichols, P.J. Shaw, and S.G. Tangye. 2006. Expansion of functionally immature transitional B cells is associated with human-immunodeficient states characterized by impaired humoral immunity. *J. Immunol.* 176:1506–1516.
- Doering, T.A., A. Crawford, J.M. Angelosanto, M.A. Paley, C.G. Ziegler, and E.J. Wherry. 2012. Network analysis reveals centrally connected genes and pathways involved in CD8⁺ T cell exhaustion versus memory. *Immunity.* 37:1130–1144. <http://dx.doi.org/10.1016/j.immuni.2012.08.021>
- Dunn-Walters, D.K., P.G. Isaacson, and J. Spencer. 1995. Analysis of mutations in immunoglobulin heavy chain variable region genes of microdissected marginal zone (MGZ) B cells suggests that the MGZ of human spleen is a reservoir of memory B cells. *J. Exp. Med.* 182:559–566. <http://dx.doi.org/10.1084/jem.182.2.559>
- Earl, L.A., and L.G. Baum. 2008. CD45 glycosylation controls T-cell life and death. *Immunol. Cell Biol.* 86:608–615. <http://dx.doi.org/10.1038/icb.2008.46>
- Ehrhardt, G.R., A. Hijikata, H. Kitamura, O. Ohara, J.Y. Wang, and M.D. Cooper. 2008. Discriminating gene expression profiles of memory B cell subpopulations. *J. Exp. Med.* 205:1807–1817. <http://dx.doi.org/10.1084/jem.20072682>
- Good, K.L., and S.G. Tangye. 2007. Decreased expression of Kruppel-like factors in memory B cells induces the rapid response typical of secondary antibody responses. *Proc. Natl. Acad. Sci. USA.* 104:13420–13425. <http://dx.doi.org/10.1073/pnas.0703872104>
- Good, K.L., D.T. Avery, and S.G. Tangye. 2009. Resting human memory B cells are intrinsically programmed for enhanced survival and responsiveness to diverse stimuli compared to naive B cells. *J. Immunol.* 182:890–901.
- Hozumi, K., N. Negishi, D. Suzuki, N. Abe, Y. Sotomaru, N. Tamaoki, C. Mailhos, D. Ish-Horowitz, S. Habu, and M.J. Owen. 2004. Delta-like 1 is necessary for the generation of marginal zone B cells but not T cells in vivo. *Nat. Immunol.* 5:638–644. <http://dx.doi.org/10.1038/ni1075>
- Kamath, B.M., R.C. Bauer, K.M. Loomes, G. Chao, J. Gerfen, A. Hutchinson, W. Hardikar, G. Hirschfield, P. Jara, I.D. Krantz, et al. 2012. NOTCH2 mutations in Alagille syndrome. *J. Med. Genet.* 49:138–144. <http://dx.doi.org/10.1136/jmedgenet-2011-100544>
- Kiel, M.J., T. Velusamy, B.L. Betz, L. Zhao, H.G. Weigelin, M.Y. Chiang, D.R. Huebner-Chan, N.G. Bailey, D.T. Yang, G. Bhagat, et al. 2012. Whole-genome sequencing identifies recurrent somatic NOTCH2 mutations in splenic marginal zone lymphoma. *J. Exp. Med.* 209:1553–1565. <http://dx.doi.org/10.1084/jem.20120910>
- Koethe, S., L. Zander, S. Köster, A. Anman, A. Ebenfelt, J. Spencer, and M. Bemark. 2011. Pivotal advance: CD45RB glycosylation is specifically regulated during human peripheral B cell differentiation. *J. Leukoc. Biol.* 90:5–19. <http://dx.doi.org/10.1189/jlb.0710404>
- Kohlhof, H., F. Hampel, R. Hoffmann, H. Burtscher, U.H. Weidle, M. Hölzel, D. Eick, U. Zimmer-Strobl, and L.J. Strobl. 2009. Notch1, Notch2, and Epstein-Barr virus-encoded nuclear antigen 2 signaling differentially affects proliferation and survival of Epstein-Barr virus-infected B cells. *Blood.* 113:5506–5515. <http://dx.doi.org/10.1182/blood-2008-11-190090>
- Kruetzmann, S., M.M. Rosado, H. Weber, U. Germing, O. Tournilhac, H.H. Peter, R. Berner, A. Peters, T. Boehm, A. Plebani, et al. 2003. Human immunoglobulin M memory B cells controlling *Streptococcus pneumoniae* infections are generated in the spleen. *J. Exp. Med.* 197:939–945. <http://dx.doi.org/10.1084/jem.20022020>
- Martin, F., and J.F. Kearney. 2002. Marginal-zone B cells. *Nat. Rev. Immunol.* 2:323–335. <http://dx.doi.org/10.1038/nri799>
- Moellerling, R.E., M. Cornejo, T.N. Davis, C. Del Bianco, J.C. Aster, S.C. Blacklow, A.L. Kung, D.G. Gilliland, G.L. Verdine, and J.E. Bradner. 2009. Direct inhibition of the NOTCH transcription factor complex. *Nature.* 462:182–188. <http://dx.doi.org/10.1038/nature08543>
- Moir, S., J. Ho, A. Malaspina, W. Wang, A.C. DiPoto, M.A. O'Shea, G. Roby, S. Kottlil, J. Arthos, M.A. Prochan, et al. 2008. Evidence for HIV-associated B cell exhaustion in a dysfunctional memory B cell compartment in HIV-infected viremic individuals. *J. Exp. Med.* 205:1797–1805. <http://dx.doi.org/10.1084/jem.20072683>
- Oberdoerffer, S., L.F. Moita, D. Neems, R.P. Freitas, N. Hacohen, and A. Rao. 2008. Regulation of CD45 alternative splicing by heterogeneous ribonucleoprotein, hnRNPL. *Science.* 321:686–691. <http://dx.doi.org/10.1126/science.1157610>

- Palanichamy, A., J. Barnard, B. Zheng, T. Owen, T. Quach, C. Wei, R.J. Looney, I. Sanz, and J.H. Anolik. 2009. Novel human transitional B cell populations revealed by B cell depletion therapy. *J. Immunol.* 182:5982–5993. <http://dx.doi.org/10.4049/jimmunol.0801859>
- Pillai, S., and A. Cariappa. 2009. The follicular versus marginal zone B lymphocyte cell fate decision. *Nat. Rev. Immunol.* 9:767–777. <http://dx.doi.org/10.1038/nri2656>
- Py, B.F., S.F. Gonzalez, K. Long, M.S. Kim, Y.A. Kim, H. Zhu, J. Yao, N. Degauque, R. Villet, P. Ymele-Leki, et al. 2013. Cochlin produced by follicular dendritic cells promotes antibacterial innate immunity. *Immunity.* 38:1063–1072. <http://dx.doi.org/10.1016/j.immuni.2013.01.015>
- Roll, P., A. Palanichamy, C. Kneitz, T. Dorner, and H.P. Tony. 2006. Regeneration of B cell subsets after transient B cell depletion using anti-CD20 antibodies in rheumatoid arthritis. *Arthritis Rheum.* 54:2377–2386. <http://dx.doi.org/10.1002/art.22019>
- Rossi, D., V. Trifonov, M. Fangazio, A. Brusca, S. Rasi, V. Spina, S. Monti, T. Vaisitti, F. Arruga, R. Famà, et al. 2012. The coding genome of splenic marginal zone lymphoma: activation of NOTCH2 and other pathways regulating marginal zone development. *J. Exp. Med.* 209:1537–1551. <http://dx.doi.org/10.1084/jem.20120904>
- Roundy, K.M., A.C. Jacobson, J.J. Weis, and J.H. Weis. 2010. The in vitro derivation of phenotypically mature and diverse B cells from immature spleen and bone marrow precursors. *Eur. J. Immunol.* 40:1139–1149. <http://dx.doi.org/10.1002/eji.200939661>
- Saito, T., S. Chiba, M. Ichikawa, A. Kunisato, T. Asai, K. Shimizu, T. Yamaguchi, G. Yamamoto, S. Seo, K. Kumano, et al. 2003. Notch2 is preferentially expressed in mature B cells and indispensable for marginal zone B lineage development. *Immunity.* 18:675–685. [http://dx.doi.org/10.1016/S1074-7613\(03\)00111-0](http://dx.doi.org/10.1016/S1074-7613(03)00111-0)
- Scheeren, F.A., M. Nagasawa, K. Weijer, T. Cupedo, J. Kirberg, N. Legendre, and H. Spits. 2008. T cell-independent development and induction of somatic hypermutation in human IgM⁺ IgD⁺ CD27⁺ B cells. *J. Exp. Med.* 205:2033–2042. <http://dx.doi.org/10.1084/jem.20070447>
- Séguin, C.A., J.S. Draper, A. Nagy, and J. Rossant. 2008. Establishment of endoderm progenitors by SOX transcription factor expression in human embryonic stem cells. *Cell Stem Cell.* 3:182–195. <http://dx.doi.org/10.1016/j.stem.2008.06.018>
- Seifert, M., and R. Küppers. 2009. Molecular footprints of a germinal center derivation of human IgM⁺(IgD⁺)CD27⁺ B cells and the dynamics of memory B cell generation. *J. Exp. Med.* 206:2659–2669. <http://dx.doi.org/10.1084/jem.20091087>
- Silva, R., S. Moir, L. Kardava, K. Debell, V.R. Simhadri, S. Ferrando-Martínez, M. Leal, J. Peña, J.E. Coligan, and F. Borrego. 2011. CD300a is expressed on human B cells, modulates BCR-mediated signaling, and its expression is down-regulated in HIV infection. *Blood.* 117:5870–5880. <http://dx.doi.org/10.1182/blood-2010-09-310318>
- Sims, G.P., R. Ettinger, Y. Shirota, C.H. Yarboro, G.G. Illei, and P.E. Lipsky. 2005. Identification and characterization of circulating human transitional B cells. *Blood.* 105:4390–4398. <http://dx.doi.org/10.1182/blood-2004-11-4284>
- Six, E.M., D. Bonhomme, M. Monteiro, K. Beldjord, M. Jurkowska, C. Cordier-Garcia, A. Garrigue, L. Dal Cortivo, B. Rocha, A. Fischer, et al. 2007. A human postnatal lymphoid progenitor capable of circulating and seeding the thymus. *J. Exp. Med.* 204:3085–3093. <http://dx.doi.org/10.1084/jem.20071003>
- Srivastava, B., W.J. Quinn III, K. Hazard, J. Erikson, and D. Allman. 2005. Characterization of marginal zone B cell precursors. *J. Exp. Med.* 202:1225–1234. <http://dx.doi.org/10.1084/jem.20051038>
- Tan, J.B., K. Xu, K. Cretegnny, I. Visan, J.S. Yuan, S.E. Egan, and C.J. Guidos. 2009. Lunatic and manic fringe cooperatively enhance marginal zone B cell precursor competition for delta-like 1 in splenic endothelial niches. *Immunity.* 30:254–263. <http://dx.doi.org/10.1016/j.immuni.2008.12.016>
- Tangye, S.G., and K.L. Good. 2007. Human IgM⁺CD27⁺ B cells: memory B cells or “memory” B cells? *J. Immunol.* 179:13–19.
- Tangye, S.G., Y.J. Liu, G. Aversa, J.H. Phillips, and J.E. de Vries. 1998. Identification of functional human splenic memory B cells by expression of CD148 and CD27. *J. Exp. Med.* 188:1691–1703. <http://dx.doi.org/10.1084/jem.188.9.1691>
- Tsuiji, M., S. Yurasov, K. Velinzon, S. Thomas, M.C. Nussenzweig, and H. Wardemann. 2006. A checkpoint for autoreactivity in human IgM⁺ memory B cell development. *J. Exp. Med.* 203:393–400. <http://dx.doi.org/10.1084/jem.20052033>
- Weill, J.C., S. Weller, and C.A. Reynaud. 2009. Human marginal zone B cells. *Annu. Rev. Immunol.* 27:267–285. <http://dx.doi.org/10.1146/annurev.immunol.021908.132607>
- Weller, S., A. Faili, G. Garcia, M.C. Braun, F. Le Deist, F. G. de Saint Basile, O. Hermine, A. Fischer, C.A. Reynaud, and J.C. Weill. 2001. CD40-CD40L independent Ig gene hypermutation suggests a second B cell diversification pathway in humans. *Proc. Natl. Acad. Sci. USA.* 98:1166–1170. <http://dx.doi.org/10.1073/pnas.98.3.1166>
- Weller, S., M.C. Braun, B.K. Tan, A. Rosenwald, C. Cordier, M.E. Conley, A. Plebani, D.S. Kumararatne, D. Bonnet, O. Tourmilhac, et al. 2004. Human blood IgM “memory” B cells are circulating splenic marginal zone B cells harboring a prediversified immunoglobulin repertoire. *Blood.* 104:3647–3654. <http://dx.doi.org/10.1182/blood-2004-01-0346>
- Weller, S., M. Mamani-Matsuda, C. Picard, C. Cordier, D. Lecoeuche, F. Gauthier, J.C. Weill, and C.A. Reynaud. 2008. Somatic diversification in the absence of antigen-driven responses is the hallmark of the IgM⁺IgD⁺CD27⁺ B cell repertoire in infants. *J. Exp. Med.* 205:1331–1342. <http://dx.doi.org/10.1084/jem.20071555>
- Wirhth, S., and A. Lanzavecchia. 2005. ABCB1 transporter discriminates human resting naive B cells from cycling transitional and memory B cells. *Eur. J. Immunol.* 35:3433–3441. <http://dx.doi.org/10.1002/eji.200535364>
- Wu, Y., C. Cain-Hom, L. Choy, T.J. Hagenbeek, G.P. de Leon, Y. Chen, D. Finkle, R. Venook, X. Wu, J. Ridgway, et al. 2010a. Therapeutic antibody targeting of individual Notch receptors. *Nature.* 464:1052–1057. <http://dx.doi.org/10.1038/nature08878>
- Wu, Y.C., D. Kipling, H.S. Leong, V. Martin, A.A. Ademokun, and D.K. Dunn-Walters. 2010b. High-throughput immunoglobulin repertoire analysis distinguishes between human IgM memory and switched memory B-cell populations. *Blood.* 116:1070–1078. <http://dx.doi.org/10.1182/blood-2010-03-275859>
- Wu, Y.C., D. Kipling, and D.K. Dunn-Walters. 2011. The relationship between CD27 negative and positive B cell populations in human peripheral blood. *Front Immunol.* 2:81. <http://dx.doi.org/10.3389/fimmu.2011.00081>
- Zandvoort, A., M.E. Lodewijk, N.K. de Boer, P.M. Dammers, F.G. Kroese, and W. Timens. 2001. CD27 expression in the human splenic marginal zone: the infant marginal zone is populated by naive B cells. *Tissue Antigens.* 58:234–242. <http://dx.doi.org/10.1034/j.1399-0039.2001.580403.x>